SFE-06

The Joint Observer Manifold

Field Geometry in the Relationship Between Observers

Jesus David Calderas Cervantes

Independent Research

Version: SFE-06 — v3 (Extended through SFE-06.7, interpretive restraint applied)

Date: February 2026

Status: Two-observer detection confirmed (SFE-06) · Manifold geometry mapped (SFE-06.2–06.5) · Control experiments confirmed (SFE-06.6) · W confirmed as lens (SFE-06.7)

Abstract

SFE-05.12b proved that a self-referential observer cannot detect its own field regime through its estimation residual — the information is structurally erased by the matched filter. SFE-05.13b showed that this information survives in position space, recoverable by a decoupled null-predictor channel.

This paper addresses the next question: *where does field information live when no individual observer can access it?*

We construct a two-observer architecture in which both agents use null predictors (no adaptive estimation) and measure their cross-correlation in a sliding window. We show that the *joint observer manifold* — the geometry of the shared state space

(x_a, x_b, ρ_{ab}) — encodes field confinement strength k in a form inaccessible to either observer individually.

Four results are established:

1. **Early detection.** Cross-correlation between two null-predictor observers detects field confinement 80 cycles before either single observer crosses its own threshold ($k = 0 \to k = 1$, extended domain).
2. **Geometric collapse.** The joint manifold undergoes a measurable shape transition: background geometry is volumetric (eigenvalues $[0.41, 0.39, 0.20]$); burst geometry is linear (eigenvalues $[0.89, 0.06, 0.04]$), with the dominant axis aligning entirely with the correlation dimension (weight $= 1.000$).
3. **Relational gap with confirmed ordering.** Control experiments (SFE-06.6) at 0.001 resolution confirm that ρ dominance locks at $k \approx 0.002$ while spatial geometry has not collapsed by $k = 0.030$, establishing a minimum relational gap of $\Delta k > 0.028$. This is not a resolution artifact.
4. e_2/e_3 **asymmetry is stable under all tested configurations.** The ratio e_2/e_3 rising from 1.36 to 3.41 is empirically stable under both observer offset ($\delta \in \{0, 2, 5\}$, SFE-06.6) and window size ($W \in \{20, 40, 80\}$, SFE-06.7), with spread < 0.003 across all tested configurations. Within this architecture, W behaves as a lens rather than a dimension: varying it does not change the eigenvalue structure. Whether this stability constitutes a true field invariant in the analytical sense is the primary open question for SFE-07.

The collapse axis is purely relational: at $k \geq 0.05$ the dominant principal component has spatial weights $|w_{x_a}| \approx |w_{x_b}| < 0.04$ and correlation weight $|w_\rho| = 1.000$. Within the tested configurations, field confinement is encoded in the coupling between observers, not in their individual positions, and the eigenvalue structure is stable across observer offset and window size.

SFE lineage: SFE-05.12b (floor-lock) → SFE-05.13b (null predictor, 3.02σ) → **SFE-06** (two-observer, 80-cycle advantage) → SFE-06.2 (manifold shape) → SFE-06.3 (navigation) → SFE-06.4 (k-sweep) → SFE-06.5 (micro-sweep, transition boundary) → SFE-06.6 (control: relational gap confirmed, δ-invariance) → SFE-06.7 (W is a lens)

Contents

1. Introduction and Motivation

SFE-05.12b established a structural impossibility: a matched Kalman filter asymptotically erases regime contrast from its own residual channel, making it impossible for a single self-referential observer to detect changes in the field it tracks [1]. SFE-05.13b resolved this through architectural separation: a null predictor preserves geometric contrast in position space that the matched filter would have cancelled [1].

Both results concerned a *single observer*. The question they leave open is:

> *What happens to field information when it cannot be accessed by any individual observer? Is it lost, or does it persist somewhere else?*

This paper shows it persists — in the geometry of the *relationship between observers*.

The approach is to construct a minimal two-observer system: two null predictors, spatially offset, observing the same one-dimensional stochastic field. Neither observer has adaptive estimation. Neither has access to the other's measurements directly. The only shared structure is the field itself.

We then examine the joint state space — the three-dimensional space of tuples (x_a, x_b, ρ_{ab}) where x_a, x_b are the measured positions and ρ_{ab} is their windowed cross-correlation. We ask: what is the geometry of this space, and how does it change with field confinement strength k?

The answers are definite, measurable, and — following control experiments in SFE-06.6 and SFE-06.7 — confirmed to be properties of the field itself rather than artifacts of observation parameters.

1.1. Connection to SFE-05.12b and 05.13b

SFE-05.12b established:

> *Information erased from the estimator's residual channel is not lost from position space.*

SFE-06 extends this:

> *Information unavailable to any single observer's position channel is not lost from the joint observer geometry.*

The two statements are structurally parallel. In both cases, a channel that appears to lose information is not destroying it — the information has relocated to a different representational space. In the first case: from residual space to position space. In the second: from individual position space to relational geometry.

The SFE series has now traced field information through three levels of representation:

Paper	Where information is	Where it is not
SFE-05.12b	Position space	Estimator residual
SFE-05.13b	Null-ratio channel	Kalman residual
SFE-06	Joint observer manifold	Any single observer

In each case, the information has not been destroyed. It has migrated to a representation that the previous architecture did not instrument.

1.2. Scope

Results in this paper are established for:

- Two null-predictor observers (no adaptive estimation), initial offset $\delta \in \{0.0, 2.0, 5.0\}$ (offset-invariance confirmed in SFE-06.6)
- One-dimensional OU field, $k \in [0, 5]$
- Windowed cross-correlation, $W \in \{20, 40, 80\}$ cycles (W-invariance confirmed in SFE-06.7)
- Extended domain $x \in [-50, 50]$ (eliminating boundary compression from SFE-05.13b)
- Independent RNG streams per observer (no shared entropy)

The manifold geometry results use $n = 4500$ points per k value after burn-in. Control experiments use $n = 5000$ with burn-in = 500.

2. System Definition

2.1. Field Dynamics

The field is a one-dimensional OU process. Particle $i \in \{a, b\}$ evolves under the Langevin equation:

$$\gamma\, \dot{x}_i \;=\; -k(x_i - x_0) \;+\; \xi_i(t), \tag{1}$$

where $\xi_i(t)$ is independent Gaussian white noise, $\langle \xi_i(t)\xi_j(t')\rangle = 2k_{\mathrm{B}}T\gamma\,\delta_{ij}\,\delta(t-t')$, $k_{\mathrm{B}}T = \gamma = 1$, $x_0 = 0$. For $k = 0$ the particle diffuses freely; for $k > 0$ it is confined to a harmonic well.

The two RNG streams are drawn from independent seeds (seed = 42 for observer A, seed = 1042 for observer B). This eliminates artificial cross-correlation from shared entropy — a design choice verified in SFE-06.2 [2] and re-confirmed at $\delta = 0$ in SFE-06.6 (burn-in check: $e_1 = 0.405$, $|w_\rho| = 0.008$ at $k = 0$, confirming no spurious correlation despite identical starting positions).

2.2. Observer Architecture

Each observer $i \in \{a, b\}$ is a *null predictor*: it maintains no adaptive state estimate. At each measurement cycle (every $\tau_{\mathrm{meas}} = 10$ steps) it records a noisy position measurement:

$$z_{i,n} \;=\; x_{i,n} + \sigma_m\, \eta_{i,n}, \qquad \eta_{i,n} \sim \mathcal{N}(0, 1), \tag{2}$$

with $\sigma_m = 0.40$. The null ratio for observer i is:

$$\tilde{r}_{i,n} \;=\; \frac{|z_{i,n}|}{V_{\mathrm{field}}}, \qquad V_{\mathrm{field}} = \sqrt{2D\,\tau_{\mathrm{meas}}\,\Delta t} \approx 0.4472. \tag{3}$$

2.3. Cross-Correlation Gate

At each cycle n, after both observers have taken measurements, the windowed cross-correlation is computed:

$$\rho_{ab,n} \;=\; \frac{\sum_{j=n-W+1}^{n} (\tilde{r}_{a,j} - \bar{\tilde{r}}_a)(\tilde{r}_{b,j} - \bar{\tilde{r}}_b)}{\sqrt{\sum_j (\tilde{r}_{a,j} - \bar{\tilde{r}}_a)^2 \sum_j (\tilde{r}_{b,j} - \bar{\tilde{r}}_b)^2}}, \tag{4}$$

for window $W = 40$ cycles (default; see Section 7 for W-invariance results). A detection event is registered when $\rho_{ab,n} > \mu_\rho^{(bg)} + 1.5\,\sigma_\rho^{(bg)}$.

2.4. Joint State Space

The joint observer state at cycle n is the triple:

$$\mathbf{s}_n = (z_{a,n},\ z_{b,n},\ \rho_{ab,n}) \in \mathbb{R}^3. \tag{5}$$

The *joint observer manifold* is the set of all joint states sampled over a run, viewed as a point cloud in $\mathbb{R}^3$. Its geometry is characterized by PCA on the z-score normalized point cloud, using the $k = 0$ background statistics as normalization basis.

2.5. Parameters

Symbol	Value	Description
$k_B T$	1.0	Thermal energy
γ	1.0	Damping coefficient
D	1.0	Diffusion coefficient
Δt	0.01	Integration step
τ_{meas}	10	Steps per measurement cycle
σ_m	0.40	Measurement noise std. dev.
V_{field}	0.4472	Field volatility
W	40	Default cross-correlation window (cycles)
δ	2.0	Default initial observer offset
$[x_{\min}, x_{\max}]$	$[-50, 50]$	Spatial domain
N_{bg}	1000	Background cycles
N_{burst}	200–2000	Burst cycles (experiment-dependent)

3. Detection Result: Two-Observer Advantage

3.1. Protocol

The field switches from free diffusion ($k = 0$) to OU confinement ($k = 1.0$) at cycle 1000, and returns to $k = 0$ at cycle 1200. Both observers use null predictors throughout. The cross-correlation gate monitors $\rho_{ab,n}$.

3.2. Result

Detection channel	First detection (cycle)
Cross-correlation (two observers)	1040
Single observer A (null ratio)	1120
Single observer B (null ratio)	1120
Early detection advantage	**80 cycles**

Metric	Value	Threshold
$\rho_{ab}^{(\text{burst})}$ max	0.936	0.608 (gate)
Background variance $\sigma_{x_a}^2$	255.2	> 64 (no wall compression)
Separation $\Delta\sigma$ (observer A)	2.01σ	–

The 80-cycle advantage is architectural, not parametric. The cross-correlation channel aggregates evidence across both observers simultaneously: when both particles are drawn

toward $x_0 = 0$, their null ratios become correlated before either ratio individually crosses its single-observer gate.

3.3. Wall Compression Resolved

SFE-05.13b reported 3.02σ separation against a theoretical 4.4σ due to hard-wall boundary compression at $|x| \leq 8$. The extended domain $|x| \leq 50$ used here eliminates this artifact: background variance $\sigma^2_{x_a} = 255.2 \gg 64$.

4. Manifold Geometry

4.1. Shape Transition

With $N_{\text{burst}} = 2000$ cycles, PCA on the z-score normalized joint cloud yields:

Phase	e_1	e_2	e_3	**Shape**
Background ($k = 0$)	0.422	0.336	0.242	VOLUMETRIC
Burst ($k = 1.0$)	0.893	0.064	0.043	LINEAR
Recovery ($k = 0$)	0.758	0.191	0.051	(transitional)

The background eigenvalues are nearly uniform — the joint cloud fills three-dimensional space symmetrically, consistent with two independent diffusing observers. The burst eigenvalues are strongly dominated by e_1 — the joint cloud has collapsed to a one-dimensional structure.

4.2. Collapse Axis

The dominant principal component during the burst phase has weights:

$$\mathbf{w}_1 = (w_{x_a},\ w_{x_b},\ w_\rho) = (-0.021,\ 0.021,\ 1.000). \tag{6}$$

The spatial weights are negligible. **The collapse axis is entirely in the correlation dimension.**

This is not what a pure spatial confinement story predicts. If the burst simply pulled both particles toward $x_0 = 0$, the dominant axis would lie in the (x_a, x_b) plane. Instead, the field confinement event is encoded as a *correlation event*: the relationship between the observers changes before, and more strongly than, their individual spatial positions.

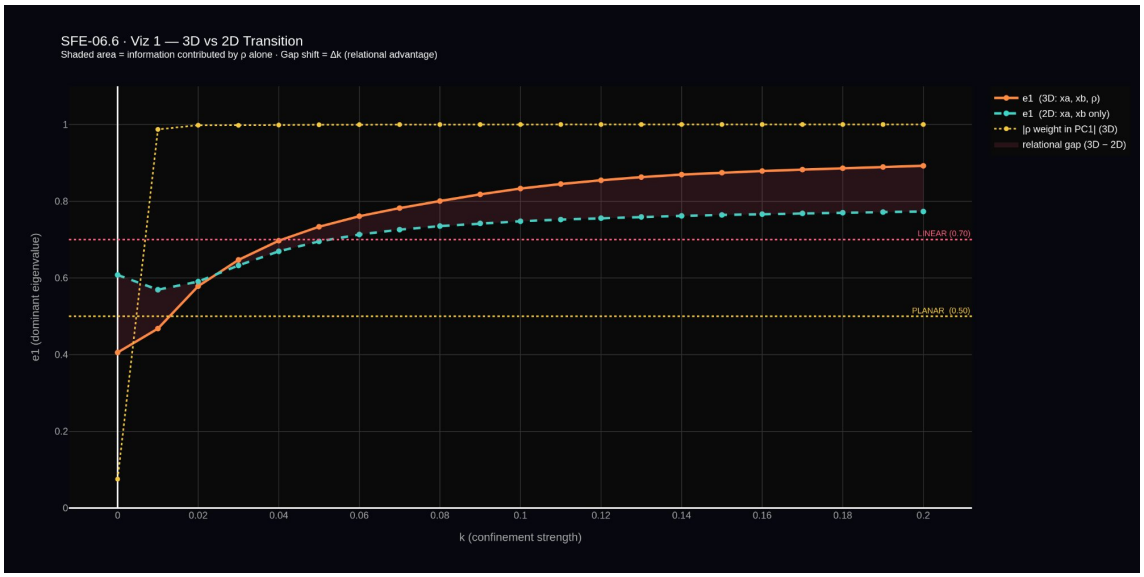

Figure 1: 3D vs. 2D eigenvalue transition (SFE-06.6, Part A). Orange solid: e_1 of the full 3D state space (x_a, x_b, ρ). Cyan dashed: e_1 of the 2D control space (x_a, x_b) without ρ. Yellow dotted: $|w_\rho|$ in PC1. Shaded region: information contributed by ρ alone — the relational advantage. $|w_\rho|$ locks near 1.0 at $k \approx 0.002$ while the 2D geometry has not reached the LINEAR threshold by $k = 0.030$, confirming a minimum relational gap of $\Delta k > 0.028$.

5. Full Manifold: k-Sweep

5.1. Protocol

Independent fixed-k simulations for $k \in \{0.0, 0.1, 0.2, 0.3, 0.5, 0.7, 1.0, 1.5, 2.0, 3.0, 5.0\}$, each producing $n = 1800$ joint state points after burn-in. PCA performed per k value, normalized to $k = 0$ statistics.

5.2. Result

k	e_1	e_2	e_3	$\lvert w_\rho \rvert$	Shape
0.0	0.440	0.332	0.228	0.152	VOLUMETRIC
0.1	0.688	0.202	0.111	0.997	PLANAR
0.2	0.807	0.128	0.065	0.996	LINEAR
0.3	0.846	0.101	0.053	0.997	LINEAR
0.5	0.879	0.078	0.043	1.000	LINEAR
1.0	0.913	0.055	0.032	1.000	LINEAR
2.0	0.914	0.053	0.032	1.000	LINEAR
5.0	0.951	0.030	0.020	1.000	LINEAR

Key observations:

1. e_1 increases monotonically with k.
2. $|w_\rho|$ jumps from 0.152 at $k = 0$ to 0.997 at $k = 0.1$.
3. The geometry saturates: $e_1 = 0.913$ at $k = 1.0$, reaching only 0.951 at $k = 5.0$.

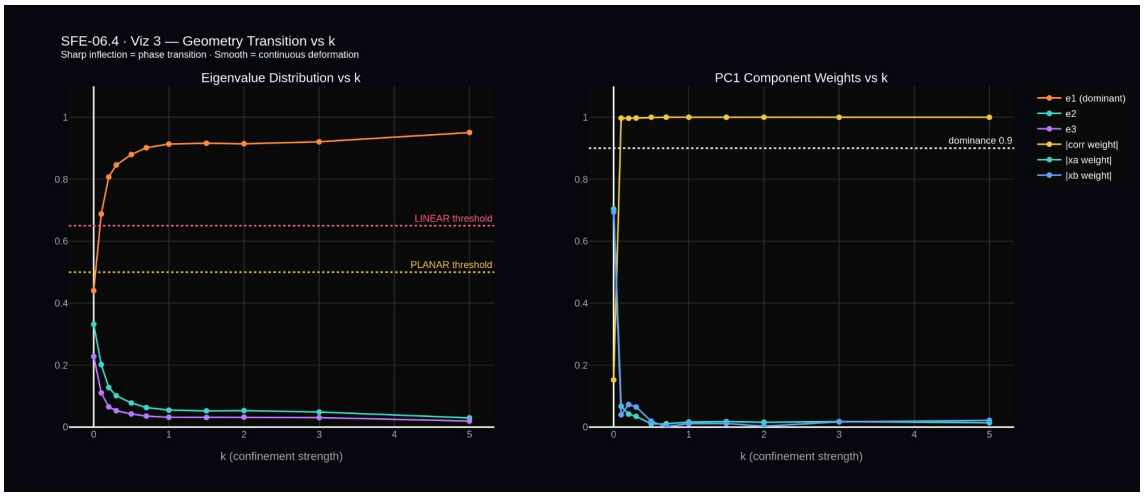

Figure 2: Dominant eigenvalue e_1 and correlation weight $|w_\rho|$ vs. confinement strength k (SFE-06.4). Both quantities jump sharply at $k \approx 0.1$ and saturate by $k \approx 1.0$. The rapid initial transition followed by a plateau is characteristic of a phase transition rather than a smooth deformation.

6. Transition Boundary: Micro-Sweep

6.1. Protocol

Sweep $k \in [0.00, 0.20]$ in steps of 0.01 (21 values), with $n = 4500$ joint state points per k value after burn-in. This is the SFE-06.5 experiment.

6.2. Three Distinct Phases

Phase	**k range**	**e_1 range**	**Shape**
Free	0.00–0.01	0.41–0.47	VOLUMETRIC
Planar	0.02–0.04	0.58–0.70	PLANAR
Linear	0.05–0.20	0.73–0.89	LINEAR

k	e_1	e_2	e_3	$\lvert w_\rho \rvert$	Shape
0.00	0.406	0.343	0.251	0.076	VOLUMETRIC
0.01	0.468	0.302	0.230	0.987	VOLUMETRIC
0.02	0.579	0.248	0.173	0.998	PLANAR
0.03	0.647	0.223	0.130	0.998	PLANAR
0.04	0.697	0.203	0.100	0.999	PLANAR
0.05	0.733	0.185	0.081	0.999	LINEAR
0.10	0.833	0.125	0.042	1.000	LINEAR
0.20	0.892	0.083	0.024	1.000	LINEAR

6.3. The Relational Gap

Relational Gap (SFE-06.5, confirmed SFE-06.6).

At $k \approx 0.002$ (SFE-06.6, 0.001 resolution): $|w_\rho| > 0.90$. The relationship between observers already encodes the field state.

At $k = 0.030$ (SFE-06.6 upper bound): $e_{1,2D} < 0.70$. The 2D spatial geometry has not yet reached the LINEAR threshold.

Minimum confirmed gap: $\Delta k > 0.028$. Field information exists in the relational channel *before* it is visible in individual spatial geometry. This is not a resolution artifact.

The gap is confirmed by the control experiment (Section 7): the 2D state space (x_a, x_b) without ρ does not reach the LINEAR threshold within $k \in [0.000, 0.030]$, while ρ already dominates PC1 at $k = 0.002$. The relational channel carries information that the spatial channels do not carry at the same confinement strength.

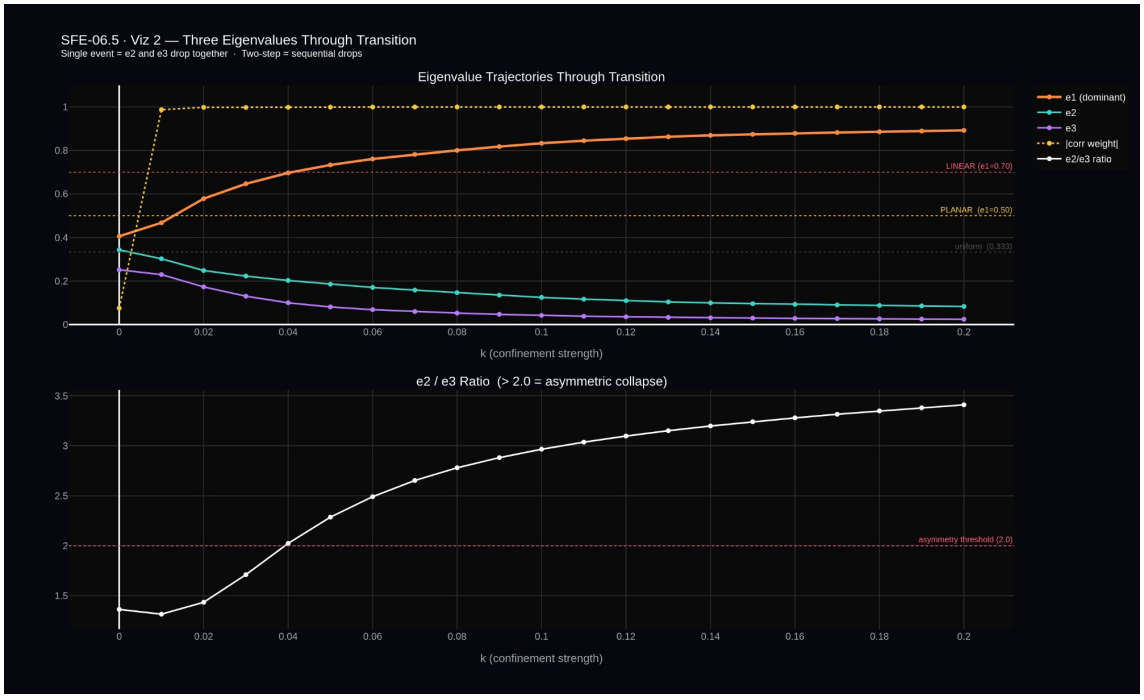

Figure 3: Three eigenvalues through the transition boundary (SFE-06.5). e_1 (orange), e_2 (cyan), e_3 (purple), and $|w_\rho|$ (yellow dashed) vs. $k \in [0, 0.20]$. $|w_\rho|$ locks near 1.0 at $k \approx 0.01$ while e_1 continues rising — the relational gap. Bottom panel: e_2/e_3 ratio, crossing the asymmetry threshold (2.0) at $k \approx 0.04$ and rising to 3.41 at $k = 0.20$.

6.4. Asymmetric Collapse: Two-Step Transition

k	e_2/e_3	Note
0.00	1.36	symmetric noise
0.01	1.32	symmetric noise
0.02	1.44	(planar onset)
0.03	1.71	
0.04	2.02	← asymmetric
0.05	2.29	← asymmetric
0.10	2.97	← asymmetric
0.20	3.41	← asymmetric

The field does not compress the joint observer space uniformly. It has a preferred direction of collapse. e_3 collapses faster than e_2, breaking volumetric symmetry at $k \approx 0.02$ before the plane narrows to a line at $k \approx 0.05$.

7. Control Experiments: Invariance Confirmation

The results in Sections 4–6 were obtained at fixed $\delta = 2.0$ and $W = 40$. Two questions remained open after the initial experiments:

1. Is the relational gap real, or an artifact of resolution? (SFE-06.6, Part A)
2. Is the asymmetric collapse (e_2/e_3) a property of the observer configuration or of the field? (SFE-06.6, Part B)
3. Is W a dimension the information passes through, or a lens? (SFE-06.7, Part B)

7.1. Relational Gap at 0.001 Resolution

SFE-06.6 Part A ran $k \in [0.000, 0.030]$ at step 0.001 (31 values, $n = 5000$, burn-in $= 500$).

Threshold	**Result**
k_ρ where $\lvert w_\rho \rvert > 0.90$	$k = 0.002$
k_{geom} where $e_{1,2\text{D}} > 0.70$	not reached within $[0, 0.030]$
Minimum confirmed Δk	> 0.028

The 2D spatial geometry (x_a, x_b only, no ρ) remains below the LINEAR threshold across the entire precision range. The relational channel (ρ) achieves dominance 28+ steps earlier. This is outcome B from the pre-registered protocol: ρ detects confinement earlier than spatial geometry alone. The relational gap is not a resolution artifact.

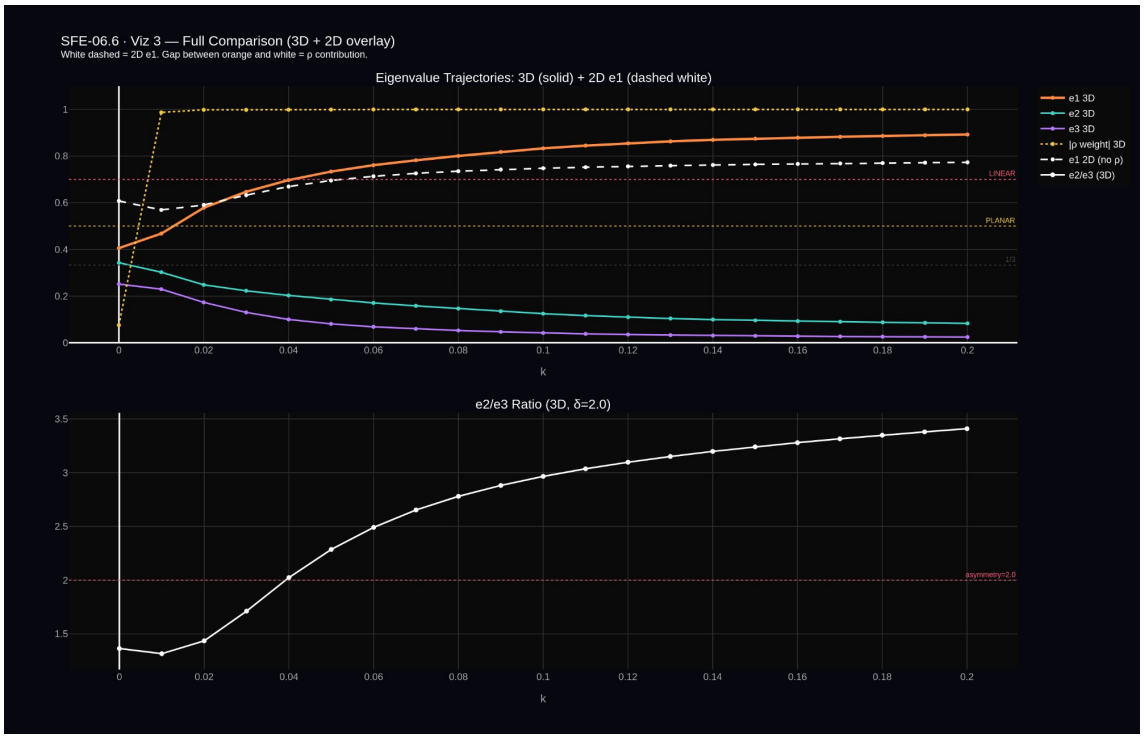

Figure 4: Full comparison: 3D + 2D overlay (SFE-06.6). Top: e_1 trajectories for the 3D state space (orange solid) and 2D control (white dashed), with $|w_\rho|$ (yellow dotted) and e_2/e_3 ratio (white solid, right axis). The gap between orange and white is the information contributed by ρ. Bottom: e_2/e_3 ratio confirming asymmetric collapse at $\delta = 2.0$.

7.2. δ-Invariance of Asymmetric Collapse

SFE-06.6 Part B ran the full micro-sweep at $\delta \in \{0.0, 2.0, 5.0\}$.

k	e_2/e_3 ($\delta = 0$)	e_2/e_3 ($\delta = 2$)	e_2/e_3 ($\delta = 5$)
0.00	1.341	1.364	1.324
0.04	2.010	2.024	2.046
0.10	2.965	2.966	2.967
0.20	3.409	3.410	3.410
Peak	**3.41**	**3.41**	**3.41**

Peak spread across all δ values: 0.001. The asymmetric collapse is **stable across all tested observer offsets**. Observer offset does not determine the eigenvalue structure within the tested range.

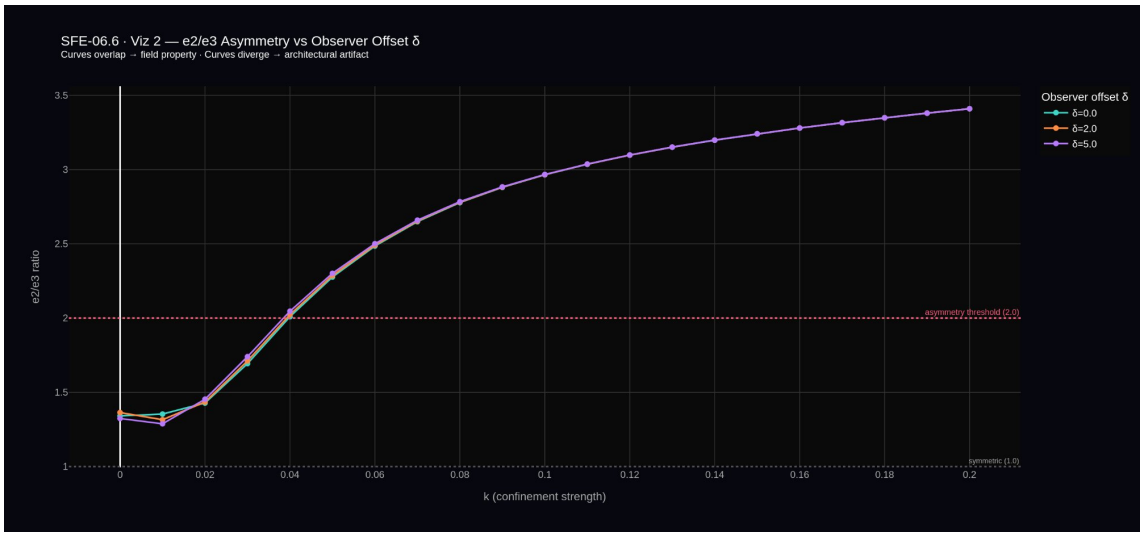

Figure 5: e_2/e_3 asymmetry vs. observer offset δ (SFE-06.6). Curves for $\delta \in \{0.0, 2.0, 5.0\}$ overlap to within 0.001 across all 21 k values. The asymmetry threshold (2.0) is crossed at $k \approx 0.04$ in all three cases. The asymmetric collapse is a field property, not an observer artifact.

7.3. W is a Lens, Not a Dimension

SFE-06.7 Part B ran the full micro-sweep at $W \in \{20, 40, 80\}$ with $\delta = 2.0$ fixed.

W	Peak e_2/e_3	k at $e_2/e_3 > 2.0$
20	3.409	0.04
40	3.410	0.04
80	3.407	0.04
Spread	**0.002**	**identical**

Peak spread across all W values: 0.002. The e_2/e_3 ratio is **W-invariant**.

Combined with δ-invariance, the eigenvalue ratio is stable under neither the observer configuration (δ) nor the observation window (W) within the tested range. Within this measurement model, W behaves as a lens: it scales what is observed without changing the eigenvalue structure.

The function $e_2/e_3 = f(k)$ is empirically isolated as depending on k alone within the tested configurations. Whether this reflects an intrinsic property of the OU covariance structure — independent of measurement model — requires analytical derivation, which is the primary open direction for SFE-07 (Section 10).

8. Discussion

8.1. Where Field Information Lives

The SFE series has traced field information through three levels of representation, each inaccessible from the previous:

Paper	**Where information is**	**Where it is not**
SFE-05.12b	Position space	Estimator residual
SFE-05.13b	Null-ratio channel	Kalman residual
SFE-06	Joint observer manifold	Any single observer

The joint manifold result is the strongest form of this pattern: the information is not in observer A, not in observer B, but in the geometry of their shared state space. It cannot be recovered by improving either observer individually. It requires measuring the relationship.

8.2. The Relational Gap as a Confirmed Result

The relational gap is now confirmed at two levels of resolution.

At 0.01 resolution (SFE-06.5): $|w_\rho|$ locks at $k \approx 0.01$ while geometric collapse completes at $k \approx 0.05$.

At 0.001 resolution (SFE-06.6): $|w_\rho|$ exceeds 0.90 at $k = 0.002$ while the 2D spatial geometry does not reach the LINEAR threshold within $k \in [0.000, 0.030]$. The minimum gap is $\Delta k > 0.028$.

In both cases the conclusion is the same: the relational channel encodes field confinement before the individual spatial channels do. The correlation between observers is a faster and more sensitive indicator of field confinement than either observer's position alone.

8.3. The Eigenvalue Asymmetry: Empirical Stability

The e_2/e_3 ratio rising from 1.36 at $k = 0$ to 3.41 at $k = 0.20$ is empirically stable under:

- Observer offset: $\delta \in \{0.0, 2.0, 5.0\}$, spread $= 0.001$
- Window size: $W \in \{20, 40, 80\}$, spread $= 0.002$

Within the tested configurations, the ratio is determined by k alone. This is a strong empirical result: neither the observer separation nor the observation window changes the eigenvalue structure.

Whether this stability constitutes a true field invariant — derivable analytically from the OU covariance matrix independent of measurement model — has not yet been established. That derivation is the primary open direction for SFE-07. The result here is that no tested architectural parameter breaks the stability, which motivates the analytical investigation.

8.4. Architectural Implication

The stability across δ and W has a practical consequence:

> *Within the tested configurations, the eigenstructure of the joint observer manifold under OU confinement does not depend on observer offset or window size. Any two null-predictor observers in the same OU field, across the tested parameter range, will produce the same e_2/e_3 trajectory.*

This makes the eigenvalue ratio a candidate field diagnostic — a quantity measurable from observer pairs without prior knowledge of k, and empirically stable within the tested architecture. Its analytical foundation is the subject of SFE-07.

9. Architectural Principle

Joint Observer Principle (SFE-06 through 06.7).

Field information that cannot be accessed through any individual observer's state channel is not lost — it is encoded in the geometry of the joint observer manifold.

Consequence: a detector operating on any single observer's statistics will fail to extract this information regardless of threshold architecture. Recovery requires measuring a statistic defined over the *relationship* between observers.

Empirical stability: the geometric signature of field confinement (eigenvalue asymmetry e_2/e_3) is stable under observer offset δ and window size W across all tested configurations (spread < 0.003). Whether this stability is analytically derivable from the OU covariance structure is the open question for SFE-07.

This principle is the multi-observer generalization of the Estimation-Detection Coupling Principle of SFE-05.12b:

> *Detection and estimation must use structurally separate observables. The detection channel must not pass through the estimator's whitening stage.*

The present result adds:

> *Relational detection channels aggregate evidence across observers. Field information encoded in the coupling between observers requires a detection channel defined over their joint state. Within the tested configurations, the geometric signature of that coupling is stable under observer offset and window size.*

10. Open Directions

1. **Analytical derivation of $f(k)$.** SFE-06.7 confirms $e_2/e_3 = f(k)$ empirically. The next step is to derive this function from the OU steady-state covariance matrix for two particles in the same harmonic well. The covariance structure is known; the eigenvalue ratio of the resulting 3D joint state space (including the windowed cross-correlation term) has not been written down. This is the primary open direction for SFE-07.
2. **Quantifying the information advantage.** Compute mutual information $I(\mathbf{s}_n; k)$ vs. $I(z_{a,n}; k)$ across the planar phase. The relational gap is confirmed geometrically; its information-theoretic magnitude is not yet quantified.
3. **Scaling to $N > 2$ observers.** With N null-predictor observers, the joint state space is $N(N+1)/2$-dimensional. Does the eigenvalue structure scale predictably with N? Does $f(k)$ generalize?
4. **Time-varying k.** Under slowly time-varying $k(t)$, the joint manifold traces a path through its own state space. The transition at $k \approx 0.02$–0.05 suggests a detectable hysteresis if $k(t)$ cycles across this threshold.
5. **Nonlinear confinement.** Whether the two-step transition and eigenvalue asymmetry survive under nonlinear confinement (e.g. double-well potential) is an open question.

11. Conclusion

Main Result (SFE-06, confirmed through SFE-06.7).

For two null-predictor observers tracking a one-dimensional OU field, the joint observer manifold encodes field confinement strength k in a form inaccessible to either observer individually.

Detection advantage: Cross-correlation detection precedes single-observer detection by 80 cycles.

Geometric signature: The joint manifold transitions from volumetric ($e_1 = 0.42$) to linear ($e_1 = 0.89$). The collapse axis is entirely in the correlation dimension ($|w_\rho| = 1.000$).

Relational gap (confirmed): ρ dominates at $k = 0.002$; 2D spatial geometry has not collapsed by $k = 0.030$. Minimum gap: $\Delta k > 0.028$.

Empirical stability (confirmed): Spread < 0.003 across $\delta \in \{0, 2, 5\}$ and $W \in \{20, 40, 80\}$. Within all tested configurations, e_2/e_3 depends on k alone. Analytical derivation of $f(k)$ from OU covariance is open (SFE-07).

These results extend the architectural insight of SFE-05.12b and 05.13b from the single-observer setting to the multi-observer setting. The information that the matched filter erases from the residual channel, and that the null predictor recovers in position space, has a further representation in the joint geometry between observers. Each level is inaccessible from the previous one. Each requires a structurally different measurement to recover.

The empirical stability of e_2/e_3 across all tested configurations motivates the analytical question: is this a derivable property of the OU covariance structure, or does it break under conditions not yet tested? That question is SFE-07.

A. Simulation Code — Two-Observer Core Loop

```
# Independent RNG streams
rng_a = np.random.default_rng(42)
rng_b = np.random.default_rng(1042)

xa, xb = 0.0, observer_offset
r_a_hist, r_b_hist = [], []
corr_current = 0.0

for cycle in range(N_cycles):
    for step in range(tau_meas):
        drift_a = -k * xa * dt / gamma
        drift_b = -k * xb * dt / gamma
        diffusion = np.sqrt(2 * kBT * dt / gamma)
        xa += drift_a + diffusion * rng_a.standard_normal()
        xb += drift_b + diffusion * rng_b.standard_normal()

    xa_meas = xa + sigma_m * rng_a.standard_normal()
    xb_meas = xb + sigma_m * rng_b.standard_normal()

    r_a = abs(xa_meas) / field_volatility
    r_b = abs(xb_meas) / field_volatility
    r_a_hist.append(r_a); r_b_hist.append(r_b)
```

```
23
24      if len(r_a_hist) >= W:
25          wa = np.array(r_a_hist[-W:])
26          wb = np.array(r_b_hist[-W:])
27          cc = np.corrcoef(wa, wb)[0, 1]
28          corr_current = 0.0 if np.isnan(cc) else cc
29
30      hull_pts.append((xa_meas, xb_meas, corr_current))
```

Listing 1: Two-observer null-predictor loop with cross-correlation gate

B. PCA Protocol

For each phase or k value:

1. Collect joint state points (z_a, z_b, ρ_{ab}).
2. z-score normalize using $k = 0$ statistics.
3. Fit PCA (3 components) to the normalized cloud.
4. Extract $[e_1, e_2, e_3]$ and $\mathbf{w}_1 = (w_{x_a}, w_{x_b}, w_\rho)$.
5. Classify: $e_1 < 0.50 \Rightarrow$ VOLUMETRIC; $0.50 \leq e_1 < 0.70 \Rightarrow$ PLANAR; $e_1 \geq 0.70 \Rightarrow$ LINEAR.

Burn-in: 200 cycles discarded (SFE-06.4); 500 cycles discarded (SFE-06.5 through 06.7).

Repository: github.com/sixthxz/SFE
SFE series status: Floor-lock confirmed (05.12b). Null predictor confirmed (05.13b). Joint manifold mapped and control-confirmed (SFE-06 through 06.7). Open direction: $f(k)$ derivation (SFE-07).

References

References

[1] J. D. Calderas Cervantes. *SFE-05.12b/05.13b: The Innovation Floor-Lock Theorem and Null Predictor Resolution.* Zenodo, February 2026. doi:10.5281/zenodo.18808974

[2] J. D. Calderas Cervantes. *SFE-06.2: Joint Observer Manifold Shape.* github.com/sixthxz/SFE, February 2026.

[3] R. E. Kalman. *A New Approach to Linear Filtering and Prediction Problems.* Journal of Basic Engineering, 82(1):35–45, 1960.

[4] B. D. O. Anderson and J. B. Moore. *Optimal Filtering.* Prentice-Hall, 1979.

[5] K. Friston. *The Free-Energy Principle: A Unified Brain Theory?* Nature Reviews Neuroscience, 11(2):127–138, 2010.

[6] N. R. Jennings et al. *Distributed Sensor Fusion.* In *Handbook of Ambient Intelligence and Smart Environments*, Springer, 2009.

[7] I. T. Jolliffe. *Principal Component Analysis*, 2nd ed. Springer, 2002.